RICE UNIVERSITY

A NUMERICAL FINITE DIFFERENCE SOLUTION TO A GAS JET IMPINGING ON A LIQUID SURFACE

by

Estrella B. Fagela-Alabastro

A THESIS SUBMITTED
IN PARTIAL FULFILLMENT OF THE
REQUIREMENTS FOR THE DEGREE OF

MASTER OF SCIENCE

Thesis Director's Signature

Houston, Texas

June, 1965

ABSTRACT

A numerical finite difference solution to the problem of a two dimensional gas jet impinging on a liquid surface at right angles has been obtained in this work. For an idealized situation of flow, the liquid surface profiles and the gas jet free streamlines were determined at several values of the parameter λ corresponding to different physical situations, the parameter λ being defined as equal to $\frac{2\rho_G V_j^2}{g_c \rho_L b}$.

The most recent significant works along this line are the experimental investigations performed by Banks and Chandrasekhara[1] and that of Olmstead[4], the latter being an analytical solution by methods of conformal mapping. Comparison of the numerical results obtained in this paper with Olmstead's results shows very good agreement for small values of λ. However, for larger values of λ corresponding to higher jet velocities, the liquid profile obtained numerically has a more complicated shape. Besides a lip, the numerical solution also shows the presence of ripples on the liquid surface. This phenomenon is supported by photographs taken during experimental runs by Banks and Chandrasekhara.

ACKNOWLEDGEMENTS

The author would like to express her sincerest appreciation to Dr. J. D. Hellums for his valuable suggestions and helpful direction of this research endeavor.

The support of the National Science Foundation under grant GP-661 is also gratefully acknowledged.

TABLE OF CONTENTS

LIST OF FIGURES

INTRODUCTION

Numerous studies had been made in the past on the behavior of jets in the vicinity of rigid boundaries. More recently, investigations have been extended to jets impinging on a deformable surface. Along this line, Banks and Chandrasekhara[1] have made significant contributions with their extensive experimental studies of the impingement and penetration of a high-velocity gas jet through a liquid surface. Their work was concerned primarily with relating the depth of the surface depression to the stagnation pressure based on the center-line velocity of the jet in the neighborhood of the liquid surface.

Among the theoretical studies on the subject, one of the most important recent works was conducted by Olmstead[4]. He considered the case of a two dimensional gas jet impinging on a liquid surface at right angles. Starting from basic fluid mechanics principles, Olmstead formulated the problem analytically, and utilizing some conformal mapping techniques, the problem was transformed to the solution of a non-linear integral equation. Finally, the liquid surface profiles and the free streamlines of the gas jet were determined utilizing some numerical solution.

An independent approach to the above-mentioned problem, which is the subject of this present investigation, is through the application of numerical finite difference methods. The ultimate goal of this study is to determine the liquid surface profiles and the gas jet free

streamlines, as Olmstead did and compare results of the two works. It is also desired to develop and evaluate a difference method for solving moving boundary-type and free streamline problems in potential flow.

STATEMENT OF THE PROBLEM

The physical representation of the problem is shown in Figure 1, page 4. In this model, the gas jet is two dimensional, symmetrical and incompressible. The source of the jet is at an infinite distance from the liquid surface. The velocity is small enough such that the effects of compressibility are negligible. The fluids (both the gas and the liquid) have small viscosities so that the frictional resistance which they exhibit may be justifiably ignored. The flow then is essentially that of an ideal jet, which is inviscid (irrotational) and incompressible. An important consequence of these assumptions is that Bernoulli's theorem becomes applicable. Finally, it is further assumed that for the jet, the gravity head is small compared to the velocity head.

For the liquid, the velocity head is assumed insignificant compared to the gravity head, the liquid has infinite dimensions and has a sufficiently high density to prohibit penetration of the impinging gas. The surface is considered to be depressed into some permanent shape, which then permits it to be treated as a streamline similar to that for flow over a solid body. Furthermore, the effect of surface tension is also ignored.

While the conditions of the problem may appear to be too idealized to be of direct practical use, it is to be appreciated that the results from this model could significantly serve as a basis for solutions of the more realistic situations wherein various factors such as compressibility and surface tension, for example, are taken into consideration.

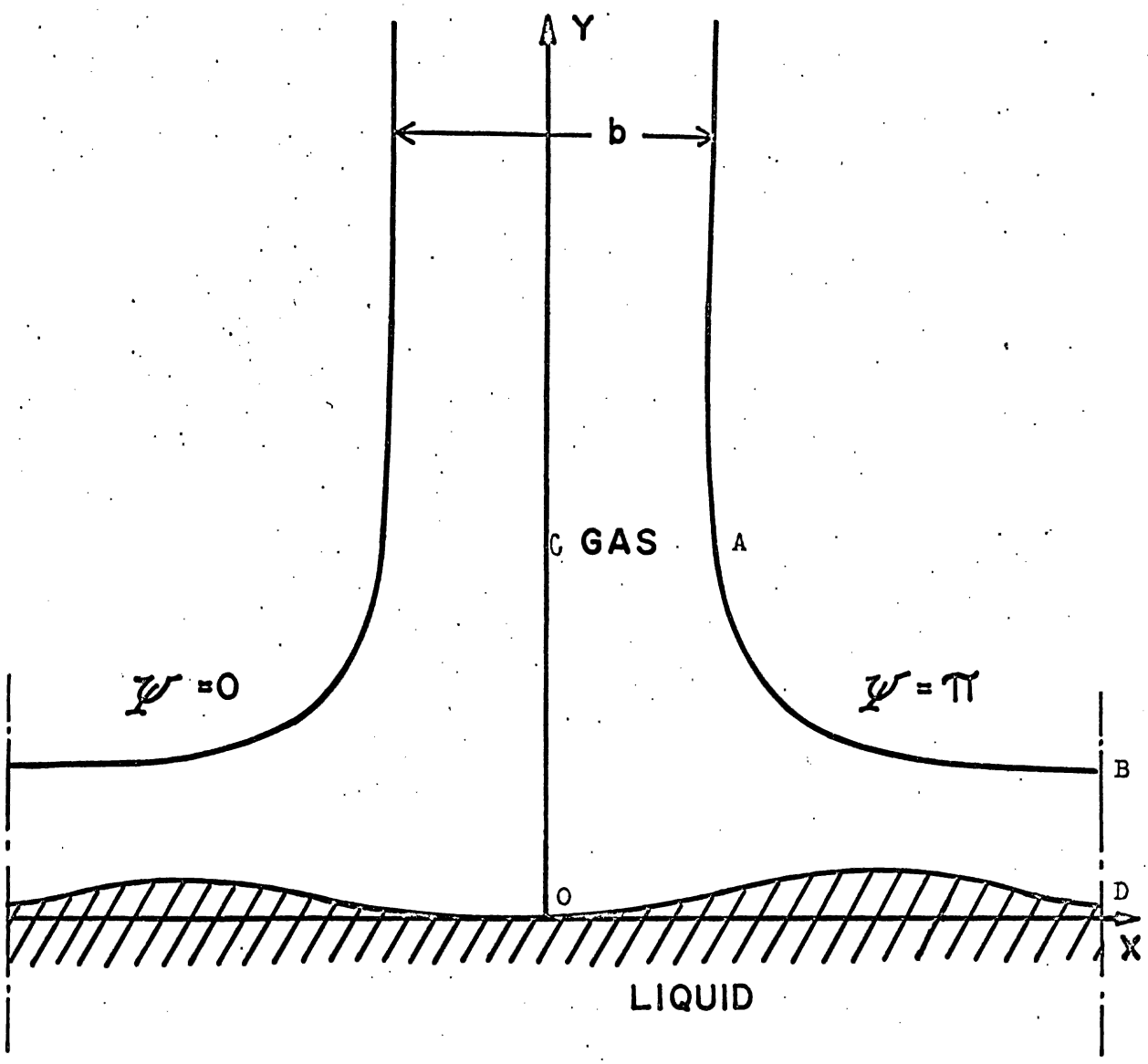

FIGURE I - A TWO DIMENSIONAL GAS JET IMPINGING ON A LIQUID SURFACE

BASIC EQUATIONS

With the physical situation defined above, the fundamental equations may now be developed.

Letting u designate the component of velocity in the x direction and v the component in the y direction, the equation of continuity for the incompressible gas flow is:

$$\frac{\partial u}{\partial x} + \frac{\partial v}{\partial y} = 0$$

The equation of motion for the gas jet reduces to:

$$\frac{1}{2 g_c}\left[u^2 + v^2\right] + \frac{P_G}{\rho_G} = \text{a constant}$$

The stream function ψ is then defined in terms of the velocity components,

$$u = \frac{\partial \psi}{\partial y} \qquad v = -\frac{\partial \psi}{\partial x}$$

such that the equation of continuity is automatically satisfied.

Since the flow is irrotational, Curl $\vec{V} = 0$

$$\frac{\partial u}{\partial y} - \frac{\partial v}{\partial x} = 0$$

Hence, if condition of irrotational flow holds:

$$\frac{\partial^2 \psi}{\partial x^2} + \frac{\partial^2 \psi}{\partial y^2} = 0$$

Any point along the free streamline may be made as reference point for the gas jet. Since for the free streamlines the velocity is constant and the pressure is atmospheric, Bernoulli's equation is written as:

$$\frac{1}{2g_c}\left[u^2 + v^2\right] + \frac{P_G}{\rho_G} = \frac{P_{atm}}{\rho_G} + \frac{1}{2g_c} V_j^2$$

where v_j is the velocity of the jet at $y = \infty$.

For the liquid, Bernoulli's equation also holds. Neglecting the velocity head,

$$\frac{P_L}{\rho_L} + y = \text{constant}$$

and taking as reference point the point $x_L = \infty$, $y_L = y_o$ the following equation results:

$$\frac{P_L}{\rho_L} + y = \frac{P_{atm}}{\rho_L} + y_o$$

At equilibrium along the liquid-gas interphase,

$$P_G = P_L$$

$$\frac{P_G - P_{atm}}{\rho_G} = \frac{1}{2g_c}\left[V_j^2 - (u^2 + v^2)\right]$$

$$\frac{P_L - P_{atm}}{\rho_L} = y_o - y$$

$$\frac{\rho_G}{2g_c}\left[V_j^2 - (u^2+v^2)\right] = \rho_L (y_o - y)$$

$$\frac{\rho_G V_j^2}{2g_c \rho_L}\left[1 - \frac{u^2+v^2}{V_j^2}\right] = y_o - y$$

Introducing the dimensionless variable, $Y = y\pi/b$, where b is the width of the jet at $y = \infty$, that is at an infinite distance from the liquid surface, the above equations can be transformed thus:

$$\frac{\rho_G V_j^2}{2\rho_L g_c}\left[1 - \frac{(u^2+v^2)}{V_j^2}\right] = \frac{b}{\pi}(Y_o - Y)$$

$$\frac{\pi \rho_G V_j^2}{2b\rho_L g_c}\left[1 - \frac{(u^2+v^2)}{V_j^2}\right] = Y_o - Y$$

At the stagnation point C, $y = 0$, and the velocity is zero. The centerline depression, Y_o is then given by:

$$Y_o = \frac{\rho_G V_j^2 \pi}{2g_c b \rho_L}$$

Defining a dimensionless parameter λ :

$$\lambda = \frac{2\rho_G V_j^2}{\rho_L g_c b}$$

Y_o may be expressed, in terms of λ, as:

$$Y_o = \frac{\pi}{4}\lambda$$

$$Y_o\left[1 - \frac{(u^2+v^2)}{V_j^2}\right] = Y_o - Y$$

$$\frac{Y}{Y_o} = \frac{u^2+v^2}{V_j^2}$$

Replacing u and v by their equivalent expression in ψ, and converting to the dimensionless variables:

$$\Psi = \frac{\pi\psi}{V_j b} \qquad X = \frac{\pi}{b}x \qquad Y = \frac{\pi}{b}y$$

$$\frac{Y}{Y_o} = \left(\frac{\partial\Psi}{\partial X}\right)^2 + \left(\frac{\partial\Psi}{\partial Y}\right)^2 = \left(\frac{\partial\Psi}{\partial\eta}\right)^2$$

In summary, the two working equations are:

$$\frac{\partial^2\Psi}{\partial X^2} + \frac{\partial^2\Psi}{\partial Y^2} = 0 \qquad (1)$$

which is applicable throughout the entire flow region including the liquid surface and the free streamlines, and

$$\frac{Y}{Y_o} = \left(\frac{\partial\Psi}{\partial X}\right)^2 + \left(\frac{\partial\Psi}{\partial Y}\right)^2 \qquad (2)$$

which holds only for the liquid surface.

BOUNDARY EQUATIONS

The stream function at the left free streamline may be arbitrarily set to $\psi = 0$, which will set the stream function of the right free streamline equal to $\psi = \pi$. By symmetry, the liquid surface will have $\psi = \frac{1}{2}\pi$.

Since flow is symmetrical, only the right region will be considered.

Referring to Figure 1, the following conditions are imposed:

On CO: $$\Psi = \frac{\pi}{2}$$

On AB: (1) $$\Psi = \pi$$

(2) $$u^2 + v^2 = V_j^2 \quad \text{or} \quad \left(\frac{\partial \Psi}{\partial X}\right)^2 + \left(\frac{\partial \Psi}{\partial Y}\right)^2 = 1$$

On OD: (1) $$\Psi = \frac{\pi}{2}$$

(2) $$\frac{Y}{Y_0} = \left(\frac{\partial \Psi}{\partial X}\right)^2 + \left(\frac{\partial \Psi}{\partial Y}\right)^2$$

The condition of plug flow at $Y = \infty$ is applied at a finite distance from the X axis, and this point is moved farther down depending on the maximum error desired. The condition of plug flow is equivalent to making the stream function linearly dependent on the axis normal to the direction of flow.

Likewise, the condition $X = \infty$, is approximated by a finite X at which plug flow is imposed.

This set of boundary conditions together with the Laplacian operator on the stream function completely defines the system whose solution will be sought by numerical techniques.

SOLUTION BY A NUMERICAL METHOD

A. Finite Difference Schemes

For the interior region, a square grid with an spacing h is chosen. Expanding $\psi(X + h, Y)$, $\psi(X - h, Y)$, $\psi(X, Y + h)$, $\psi(X, Y - h)$ about the point (X, Y) in the Taylor Series:

$$\Psi(X+h, Y) = \Psi(X, Y) + h\left(\frac{\partial \Psi}{\partial X}\right)_{X,Y} + \frac{h^2}{2!}\left(\frac{\partial^2 \Psi}{\partial X^2}\right)_{X,Y}$$

$$+ \frac{h^3}{3!}\left(\frac{\partial^3 \Psi}{\partial X^3}\right)_{X,Y} + \frac{h^4}{4!}\left(\frac{\partial^4 \Psi}{\partial X^4}\right)(\eta_1) \qquad (1)$$

where:

$$X \leq \eta_1 \leq X + h$$

$$\Psi(X-h, Y) = \Psi(X, Y) - h\left(\frac{\partial \Psi}{\partial X}\right)_{X,Y} + \frac{h^2}{2!}\left(\frac{\partial^2 \Psi}{\partial X^2}\right)_{X,Y}$$

$$- \frac{h^3}{3!}\left(\frac{\partial^3 \Psi}{\partial X^3}\right)_{X,Y} + \frac{h^4}{4!}\left(\frac{\partial^4 \Psi}{\partial X^4}\right)(\eta_2) \qquad (2)$$

where:

$$X - h \leq \eta_2 \leq X$$

$$\Psi(X, Y+h) = \Psi(X, Y) + h\left(\frac{\partial \Psi}{\partial Y}\right)_{X,Y} + \frac{h^2}{2!}\left(\frac{\partial^2 \Psi}{\partial Y^2}\right)_{X,Y}$$

$$+ \frac{h^3}{3!}\left(\frac{\partial^3 \Psi}{\partial Y^3}\right)_{X,Y} + \frac{h^4}{4!}\left(\frac{\partial^4 \Psi}{\partial Y^4}\right)(\gamma_1) \qquad (3)$$

where: $Y \le \gamma_1 \le Y + h$

$$\Psi(X, Y-h) = \Psi(X,Y) - h\left(\frac{\partial \Psi}{\partial Y}\right)_{X,Y} + \frac{h^2}{2!}\left(\frac{\partial^2 \Psi}{\partial Y^2}\right)_{X,Y}$$

$$- \frac{h^3}{3!}\left(\frac{\partial^3 \Psi}{\partial Y^3}\right)_{X,Y} + \frac{h^4}{4!}\left(\frac{\partial^4 \Psi}{\partial Y^4}\right)(\gamma_2) \qquad (4)$$

where: $Y - h \le \gamma_2 \le Y$

Adding equations (1) and (2), there is obtained:

$$h^2\left(\frac{\partial^2 \Psi}{\partial X^2}\right)_{X,Y} = \Psi(X+h, Y) + \Psi(X-h, Y) - 2\Psi(X,Y)$$

$$- \frac{h^4}{4!}\left[\left(\frac{\partial^4 \Psi}{\partial X^4}\right)(\eta_1) + \left(\frac{\partial^4 \Psi}{\partial X^4}\right)(\eta_2)\right] \qquad (5)$$

Addition of equations (3) and (4) yields:

$$h^2\left(\frac{\partial^2 \Psi}{\partial Y^2}\right) = \Psi(X, Y+h) + \Psi(X, Y-h) - 2\Psi(X,Y)$$

$$- \frac{h^4}{4!}\left[\left(\frac{\partial^4 \Psi}{\partial Y^4}\right)(\gamma_1) + \left(\frac{\partial^4 \Psi}{\partial Y^4}\right)(\gamma_2)\right] \qquad (6)$$

Finally, an approximation to the Laplace equation is obtained by combining equations (5) and (6) above. This is of order 2 in h, and is the well-known 5-point

finite difference analogue to the Laplace equation. It has been proven by Greenspan[3] that there is no other finite difference scheme involving only five points with a higher order of error.

$$\left(\frac{\partial^2\Psi}{\partial X^2}\right)_{X,Y} + \left(\frac{\partial^2\Psi}{\partial Y^2}\right)_{X,Y} - \frac{1}{h^2}\left[\Psi(x+h, Y) + \Psi(x-h, Y) + \Psi(X, Y+h) + \Psi(X, Y-h) - 4\Psi(X,Y)\right] = -\frac{h^2}{4!}\left[2\left(\frac{\partial^4\Psi}{\partial X^4}\right)(\bar{\eta}) + 2\left(\frac{\partial^4\Psi}{\partial Y^4}\right)(\bar{\gamma})\right]$$

where:

$$x-h \leq \bar{\eta} \leq x+h$$

$$Y-h \leq \bar{\gamma} \leq Y+h$$

To simplify the notations, the Laplacian operator is denoted by the symbol ∇^2 and L (ψ) represents

$$L(\Psi) = \Psi(x+h, Y) + \Psi(x-h, Y) + \Psi(X, Y+h) + \Psi(X, Y-h) - 4\Psi(X, Y)$$

The bound for the error of the operator L (ψ) is given by:

$$\left| \nabla^2\Psi - \frac{L(\Psi)}{h^2} \right| \leq \frac{h^2}{6} M_4$$

where: $$M_K = \underset{I}{\text{Sup}} \left| \frac{\partial^K \Psi}{\partial x^P \partial y^q} \right|$$

" I " represents the square region containing all the five points involved.

The above development applies only to the solution domain far from the curved boundaries. At regions adjacent to the boundaries, however, spacings are inherently irregular, and the appropriate finite difference schemes are much more complicated.

For the points near the curved boundaries, two cases are considered:

Case 1: One regular grid line passing through the point (X, Y) cuts the curved boundary.

To illustrate, the point (X, Y - ξ h) is assumed to be the point of intersection between the grid line and the boundary. Again, expanding $\psi(X, Y - \xi h)$ about $\psi(X, Y)$:

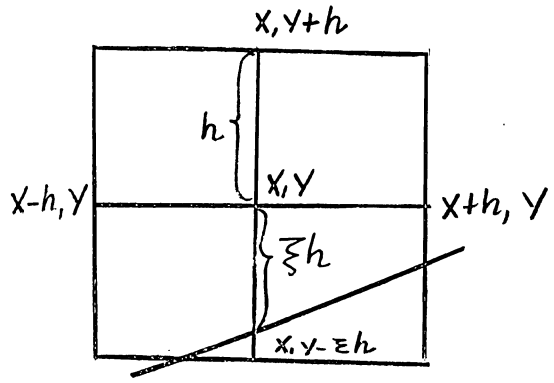

$$\Psi(X, Y-\xi h) = \Psi(X,Y) - (\xi h)\left(\frac{\partial \Psi}{\partial Y}\right)_{X,Y} + \frac{(\xi h)^2}{2!}\left(\frac{\partial^2 \Psi}{\partial Y^2}\right)_{X,Y}$$

$$- \frac{(\xi h)^3}{3!}\left(\frac{\partial^3 \Psi}{\partial Y^3}\right)_{X,Y} + \frac{(\xi h)^4}{4!}\left(\frac{\partial^4 \Psi}{\partial Y^4}\right)(\gamma_1)$$

where: $Y - \xi h \leq \gamma_1 \leq Y$

The above equation is combined with the Taylor Series expansion for $\psi(X, Y + h)$ to yield the following:

$$\left[\frac{\Psi(X,Y+h)-\Psi(X,Y)}{h} + \frac{\Psi(X,Y-\xi h)-\Psi(X,Y)}{\xi h}\right] = \frac{1}{2}(h+\xi h)\left(\frac{\partial^2\Psi}{\partial Y^2}\right)_{X,Y}$$

$$+\frac{1}{3!}\left[h^2-(\xi h)^2\right]\left(\frac{\partial^3\Psi}{\partial Y^3}\right)(\bar{\gamma}) + \frac{1}{4!}\left[h^3+(\xi h)^3\right]\left(\frac{\partial^4\Psi}{\partial Y^4}\right)(\bar{\gamma})$$

where: $Y-\xi h \le \bar{\gamma} \le Y+h$

$$\left(\frac{\partial^2\Psi}{\partial Y^2}\right)_{X,Y} = \frac{2}{h^2(1+\xi)}\left[\Psi(X,Y+h)-\Psi(X,Y)+\frac{\Psi(X,Y-\xi h)-\Psi(X,Y)}{\xi}\right]$$

$$-\frac{2h^2}{3!h}\left[1-\xi\right]\left(\frac{\partial^3\Psi}{\partial Y^3}\right)(\bar{\gamma}) - \frac{2h^3}{4!h}\left[1-\xi+\xi^2\right]\left(\frac{\partial^4\Psi}{\partial Y^4}\right)(\bar{\gamma})$$

The expression for the second partial in X is the same as that for the square grid. For this particular case, the operator L (ψ) will assume the following form:

$$L(\Psi) = \frac{2}{1+\xi}\left[\Psi(X,Y+h)-\Psi(X,Y)+\frac{\Psi(X,Y-\xi h)-\Psi(X,Y)}{\xi}\right]$$

$$+\left[\Psi(X+h,Y)+\Psi(X-h,Y)-2\Psi(X,Y)\right]$$

In this case, the error is bounded by:

$$\left|\nabla^2\Psi - \frac{L(\Psi)}{h^2}\right| \le \frac{2h}{3!}(1-\xi)M_3 + \frac{2}{4!}h^2(1-\xi+\xi^2)M_4$$

It is to be noted that the bound for uneven grid spacing has a lower order than that for the square grid although the same number of points is involved.

Case 2: Two grid lines emanating from the point (X, Y) cut the curved boundary.

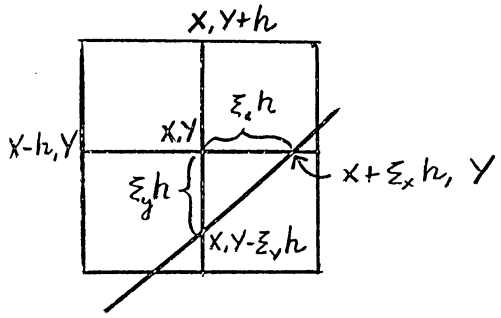

The two points of intersection are denoted by $(X + \xi_x h, Y)$ and $(X, Y - \xi_y h)$. As in the previous analyses, the Taylor series expansions for the stream function of the four pertinent points are written about the point (X, Y). An approximation to the Laplacian operator is then obtained by the combination of these expansions. $L(\psi)$, the finite difference approximation to the Laplacian operator is derived as:

$$L(\Psi) = \frac{2}{\xi_x(1+\xi_x)}\left[\xi_x \Psi(X-h, Y) + \Psi(X+\xi_x h, Y) - \Psi(X,Y)[1+\xi_x]\right]$$

$$+ \frac{2}{\xi_y(1+\xi_y)}\left[\xi_y \Psi(X, Y+h) + \Psi(X, Y-\xi_y h) - \Psi(X,Y)(1+\xi_y)\right]$$

The maximum difference between $\nabla^2\psi$ and L (ψ) is:

$$\left|\nabla^2\Psi - \frac{L(\Psi)}{h^2}\right| \leq \left| \frac{2}{3!} h(\xi_x - 1) M_3 + \frac{2}{4!} h^2(\xi_x^2 - \xi_x + 1) M_4 + \frac{2h}{3!}(1 - \xi_y) M_3 + \frac{2h^2}{4!}(1 - \xi_y + \xi_y^2)\right|$$

$$\left|\nabla^2\Psi - \frac{L(\Psi)}{h^2}\right| \leq \frac{2h}{3!}|\xi_x - \xi_y| M_3 + \frac{2}{4!}\left|2 - (\xi_x + \xi_y) + \xi_x^2 + \xi_y^2\right| M_4$$

B. Method of Solution

The flow region is subdivided into grid spaces using a finer mesh near the liquid surface since the above analyses show that the operator used for points adjacent to the curved boundary is of lower order than that for the square mesh.

A Gauss-Seidel iteration technique is utilized in which the most recently computed values are used to solve for the neighboring points. This method necessitates a trial solution covering the entire flow region.

The starting solution taken for the free streamline is that for a jet impinging on a flat plate which has been solved by Milne-Thomson[5]. Its position in the flow region is given by the equation:

$$Y = \frac{\pi}{2}\left(1 + \frac{\lambda}{2}\right) + \log \coth\left[\frac{X}{2} - \frac{\pi}{4}\right]$$

The depression at the center-line, Y_o , is known for any value of the parameter λ . As a trial solution for the liquid profile for $\lambda = 0.10$, a straight line from the minimum point passing through the point representing X_∞ is used. For higher values of λ , the liquid profile determined corresponding to the higher previous value of the parameter, is used as starting solution.

With the liquid surface fixed at the trial profile, the points on the first grid line parallel to the X-axis are determined by means of the appropriate operator for points adjacent to a curved line. The condition that all points on the boundary have values of stream function equal to $\frac{\pi}{2}$ is imposed.

After the entire first line is determined, computation proceeds to the next line and now employs equations for the square grid. The succeeding lines are determined in similar manner always proceeding in an orderly fashion from left to right.

At the points near the free streamline, the scheme for uneven grid spacing (Case 1 or 2, whichever is applicable) is employed.

Now with the liquid profile and the free streamline fixed, the entire flow region is iterated on until the stream function for each point satisfies a set criterion for convergence.

The pressure distribution at the grid lines along the liquid surface is then calculated using the equation:

$$\mathcal{J}_G = \frac{P_G - P_{atm}}{\frac{1}{2g_c}\rho_G V_j^2} = 1 - \left(\frac{\partial \Psi}{\partial X}\right)^2 + \left(\frac{\partial \Psi}{\partial Y}\right)^2 = 1 - \left(\frac{\partial \Psi}{\partial \eta}\right)^2$$

where η is a unit vector normal to the curved boundary.

Referring to the representation shown below, the following development is made:

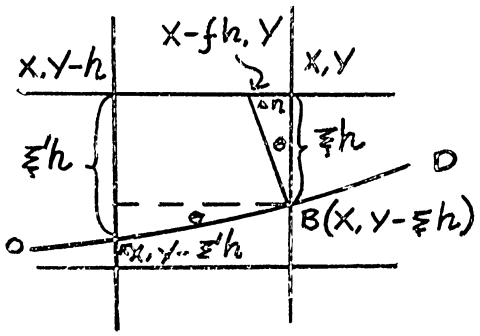

Expansion is made on $\psi(X - fh, Y)$ about the point B in the curve OD in a Taylor Series:

$$\Psi(x-fh,y) = \Psi_B + \Delta n\left(\frac{\partial \Psi}{\partial n}\right) + \frac{(\Delta n)^2}{2!}\frac{\partial^2 \Psi}{\partial n^2} + \frac{(\Delta n)^3}{3!}\frac{\partial^3 \Psi}{\partial n^3} \quad (8)$$

Since Laplace's equation also applies to the boundaries and the liquid surface is considered a streamline, $\frac{\partial^2 \Psi}{\partial \eta^2} = 0$ on the liquid surface.

$$\left(\frac{\partial \Psi}{\partial \eta}\right)_B = \frac{\Psi(X-fh,Y) - \Psi_B}{\Delta n} - \frac{(\Delta n)^3}{3!}\frac{\partial^3 \Psi}{\partial \eta^3} \quad (8)$$

$$\left|\left(\frac{\partial \Psi}{\partial \eta}\right)_B - \left\{\frac{\Psi(X-fh,Y) - \Psi_B}{\Delta n}\right\}\right| \leq \frac{\Delta n^2}{3!} M_3$$

Evaluating $\psi(X - fh, Y)$ by linear interpolation involving points $\psi(X, Y)$ and $\psi(X, Y - h)$:

$$\Psi(X-fh, Y) = \Psi(X,Y) + f_1\left[\Psi(X, Y-h) - \Psi(X,Y)\right]$$

Evaluation of Δ n:

A straight line between two adjacent points along the curve is assumed, and the angle θ which the normal makes with the vertical determined.

$$\tan\theta = (\xi' - \xi)$$

Hence,

$$f = \xi(\xi' - \xi)$$

$$(\Delta n)^2 = h^2\left[f^2 + \xi^2\right]$$

$$= h^2\xi^2\left[1 + (\xi' - \xi)^2\right]$$

$$\eta_G = 1 - \left(\frac{\partial \Psi}{\partial \eta}\right)^2 = 1 - \frac{\left[\Psi(x,y) + f\left[\Psi(x, y-h) - \Psi(x,y)\right] - \Psi_B\right]^2}{h^2\xi^2(1 + (\xi' - \xi)^2)}$$

Then, applying the equilibrium condition,

$$\eta_G = 1 - \frac{Y}{Y_0}$$

Y can be evaluated. In this manner, a new liquid surface profile is determined.

The entire procedure is repeated as many times as necessary until the maximum change in the position of liquid surface has met a set criterion of convergence.

A similar method is followed to determine the position of the free streamline. Keeping the position of the liquid surface fixed at the position determined by the method described above, the pressures are calculated on the free streamlines and points near it. The scheme used to calculate the pressure along the free streamline is the same as that for the liquid profile.

As previously mentioned, points adjacent to the curved streamline are of two kinds:

Case 1: A regular grid line cuts the surface at a point, e.g., (X + ξh, Y)

Case 2: Two grid lines cut the surface at points such as (X + ξ_xh, Y) and (X, Y + ξ_yh).

For the first case, the expressions for $\frac{\partial \Psi}{\partial X}$ and $\frac{\partial \Psi}{\partial Y}$ are needed. Expanding $\psi(X + \xi h, Y)$ and $Y(X - h, Y)$ in a Taylor Series about the point (X, Y)

$$\Psi(X+\xi h, Y) = \Psi(X,Y) + (\xi h)\left(\frac{\partial \Psi}{\partial X}\right)_{X,Y} + \frac{(\xi h)^2}{2}\left(\frac{\partial^2 \Psi}{\partial X^2}\right)_{X,Y} + \frac{(\xi h)^3}{3!}\left(\frac{\partial^3 \psi}{\partial X^3}\right)(\eta_1)$$

$$X \le \eta_1 \le X + \xi h \qquad (7)$$

$$\Psi(X-h, Y) = \Psi(X,Y) - h\left(\frac{\partial \Psi}{\partial X}\right)_{X,Y} + \frac{h^2}{2!}\left(\frac{\partial^2 \Psi}{\partial X^2}\right)_{X,Y} - \frac{h^3}{3!}\left(\frac{\partial^3 \Psi}{\partial X^3}\right)(\eta_2)$$

$$X - h \le \eta_2 \le X \qquad (8)$$

Subtracting equation (8) from (7), the expression for $\left(\frac{\partial \Psi}{\partial X}\right)_{X,Y}$ is obtained.

$$\left(\frac{\partial \Psi}{\partial X}\right)_{X,Y} = \frac{\left(\frac{1}{\xi}\right)\left[\Psi(X+\xi h, Y) - \Psi(X,Y)\right] + \xi\left[\Psi(X,Y) - \Psi(X-h,Y)\right]}{h(1+\xi)}$$

$$- \frac{\xi h^2}{3!(1+\xi)}\left[\left(\frac{\partial^3 \Psi}{\partial X^3}\right)M_1 + \left(\frac{\partial^3 \Psi}{\partial Y^3}\right)M_2\right]$$

Let

$$\Delta_X = \frac{\frac{1}{\xi}\left[\Psi(X+\xi h, Y) - \Psi(X,Y)\right] + \xi\left[\Psi(X,Y) - \Psi(X-h,Y)\right]}{h(1+\xi)}$$

The following error bound is thus obtained:

$$\left| \left(\frac{\partial \Psi}{\partial X}\right)_{X,Y} - \Delta_X \right| \leq \frac{\xi h^2}{6} M_3$$

In a similar manner, expanding $\psi(X, Y + h)$ and $\psi(X, Y - h)$ in a Taylor Series and subtracting the latter from the former, a finite difference approximation for $\left(\frac{\partial \Psi}{\partial Y}\right)_{X,Y}$ is obtained:

$$\Delta_y = \frac{\Psi(X, Y+h) - \Psi(X, Y-h)}{2h}$$

The error is bounded as follows:

$$\left| \left(\frac{\partial \Psi}{\partial Y}\right)_{X-Y} - \Delta_y \right| \leq \frac{h^2}{6} M_3$$

Now treating the second case:

Δ_x is seen to be the same as for the first case;

while Δ_y is given by

$$\Delta_y = \frac{\frac{1}{\xi_y}\left[\Psi(X, Y+\xi_y h)-\Psi(X,Y)\right]+\xi_y\left[\psi(X,Y)-\Psi(X,Y-h)\right]}{h(1+\xi_y)}$$

$$-\frac{\xi_y h^2}{3!(1+\xi_y)}\left[\frac{\partial^3\Psi}{\partial y^3}(\eta_1)+\frac{\partial^3\Psi}{\partial y^3}(\eta_2)\right]$$

resulting in the following error bound:

$$\left|\left(\frac{\partial\Psi}{\partial y}\right)_{x,y}-\Delta_y\right| \leq \frac{\xi_y h^2}{3!} M_3$$

For both cases, the pressure expression is

$$\mathcal{P}_G = 1-\left[\Delta_x^2+\Delta_y^2\right]$$

Points which are sufficiently far from the boundary such that they lie on a square grid are simply special cases of the above, for which $\xi = 1$.

The position of the line at which $\mathcal{P} = 0$, which is the free streamline, is then determined by inverse interpolation in which Langrange's formula was employed, as follows:

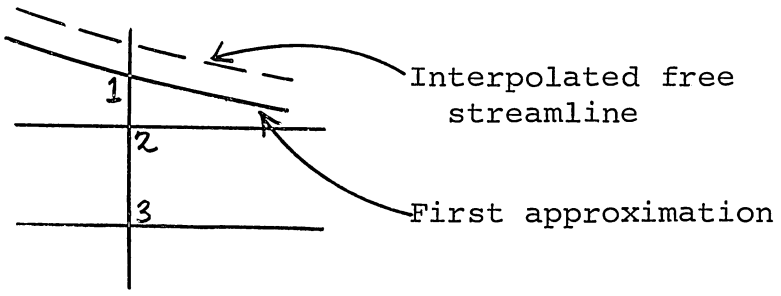

$$Y_0 = \frac{(\Psi_0-\Psi_2)(\Psi_0-\Psi_3)}{(\Psi_1-\Psi_2)(\Psi_1-\Psi_3)} Y_1 + \frac{(\Psi_0-\Psi_1)(\Psi_0-\Psi_3)}{(\Psi_2-\Psi_1)(\Psi_2-\Psi_3)} Y_2$$

$$+ \frac{(\Psi_0-\Psi_1)(\Psi_0-\Psi_2)}{(\Psi_3-\Psi_1)(\Psi_3-\Psi_2)} Y_3$$

This newly determined position of the free streamline thus enables the calculation of a new set of values for the function of points within the region. As in the solution for the liquid profile, iteration is carried out until convergence is attained. The procedure is repeated until the position of the free streamline no longer changes. Then corrections are made on the liquid profile by repeating the procedure from the beginning.

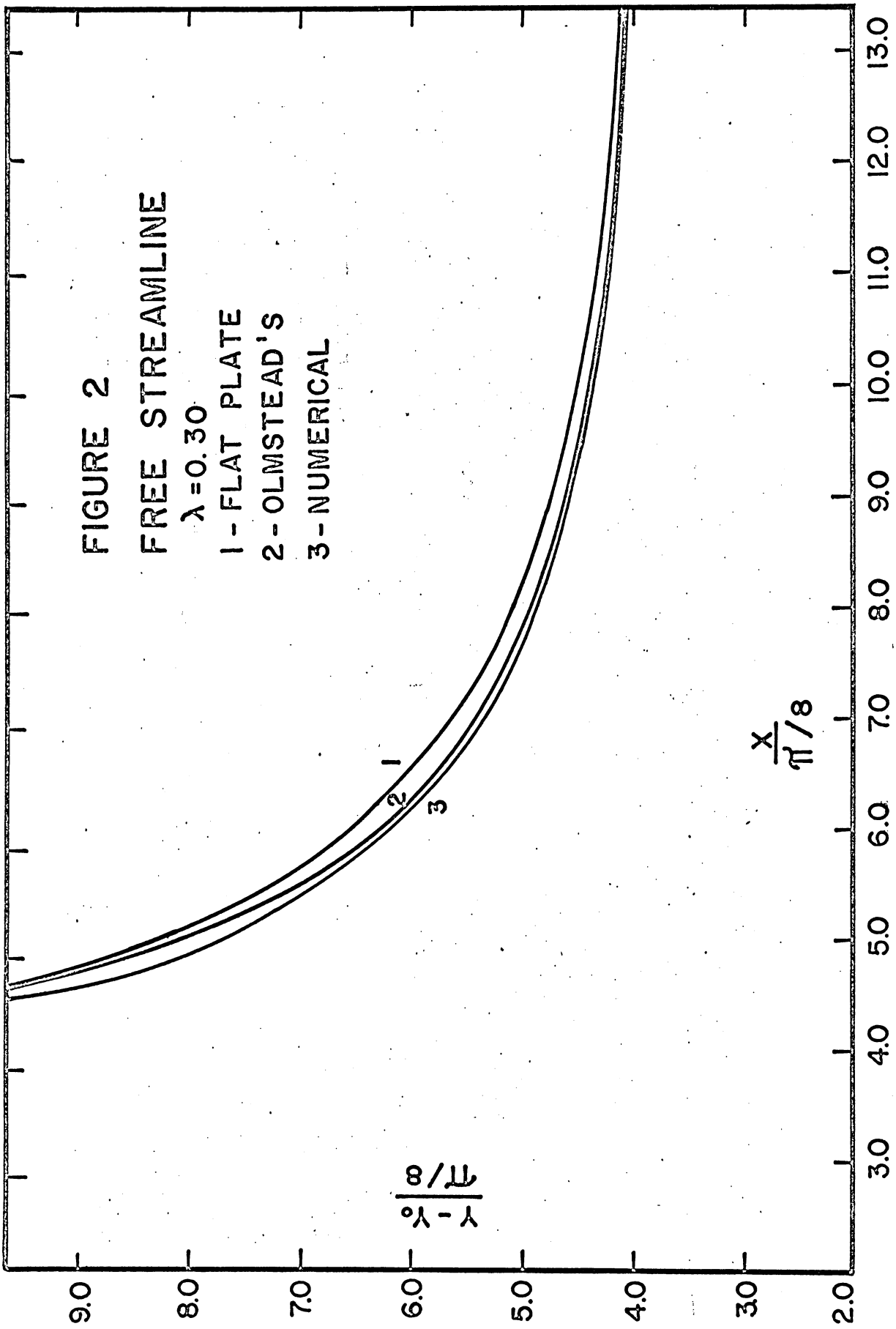
FIGURE 2
FREE STREAMLINE
λ=0.30
1 - FLAT PLATE
2 - OLMSTEAD'S
3 - NUMERICAL
1
2
3
$\frac{\psi - \psi_0}{\pi/8}$
$\frac{x}{\pi/8}$
9.0
8.0
7.0
6.0
5.0
4.0
3.0
2.0
3.0
4.0
5.0
6.0
7.0
8.0
9.0
10.0
11.0
12.0
13.0

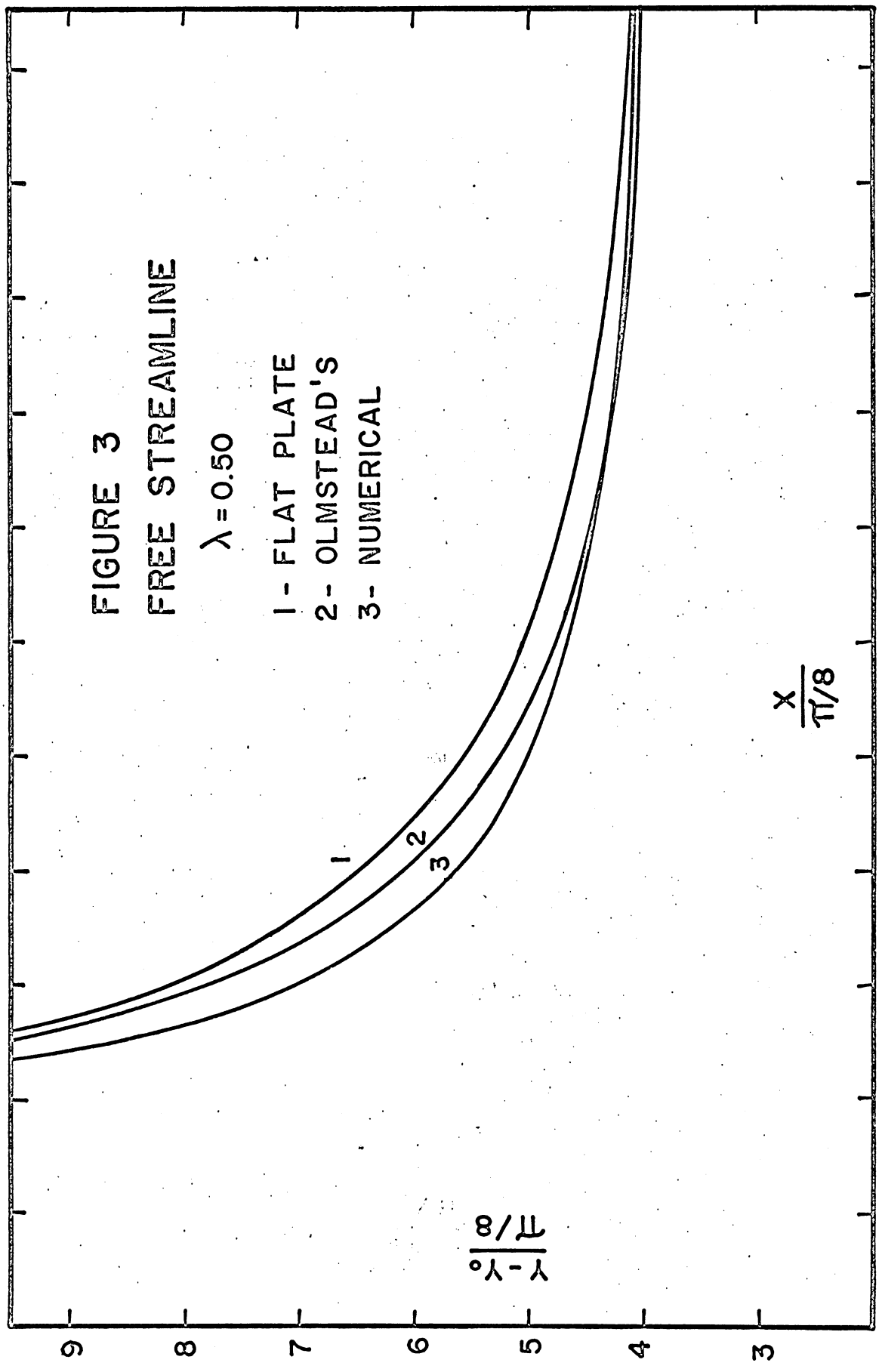
FIGURE 3
FREE STREAMLINE
λ = 0.50
1 - FLAT PLATE
2 - OLMSTEAD'S
3 - NUMERICAL
1
2
3
$\frac{\psi - \psi_0}{\pi/8}$
$\frac{x}{\pi/8}$
2
3
4
5
6
7
8
9
10
11
12
13

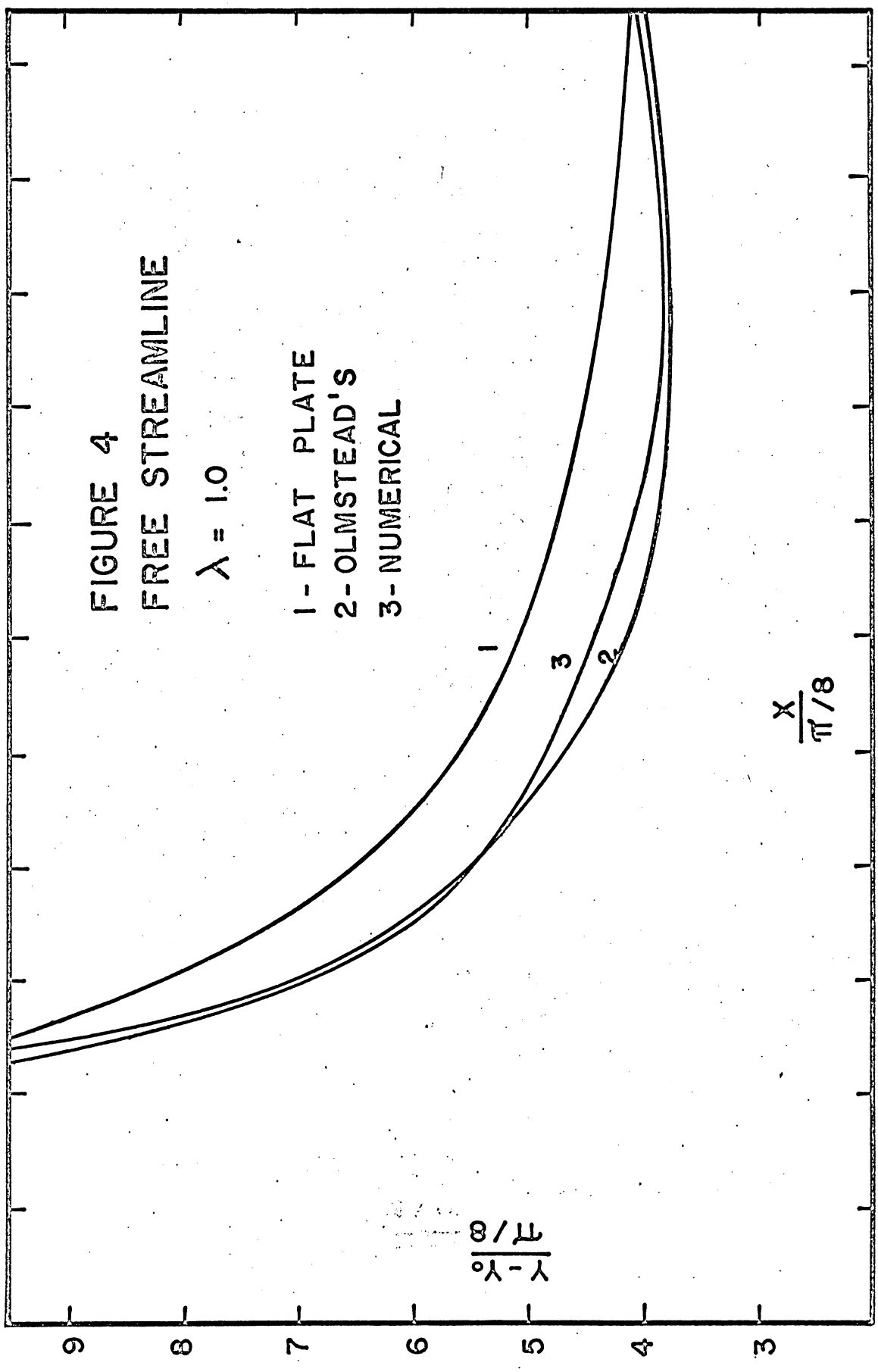
FIGURE 4
FREE STREAMLINE
λ = 1.0
1- FLAT PLATE
2- OLMSTEAD'S
3- NUMERICAL
1
2
3
$\frac{\psi - \psi_0}{\pi/8}$
$\frac{x}{\pi/8}$
2
3
4
5
6
7
8
9
10
11
12
13

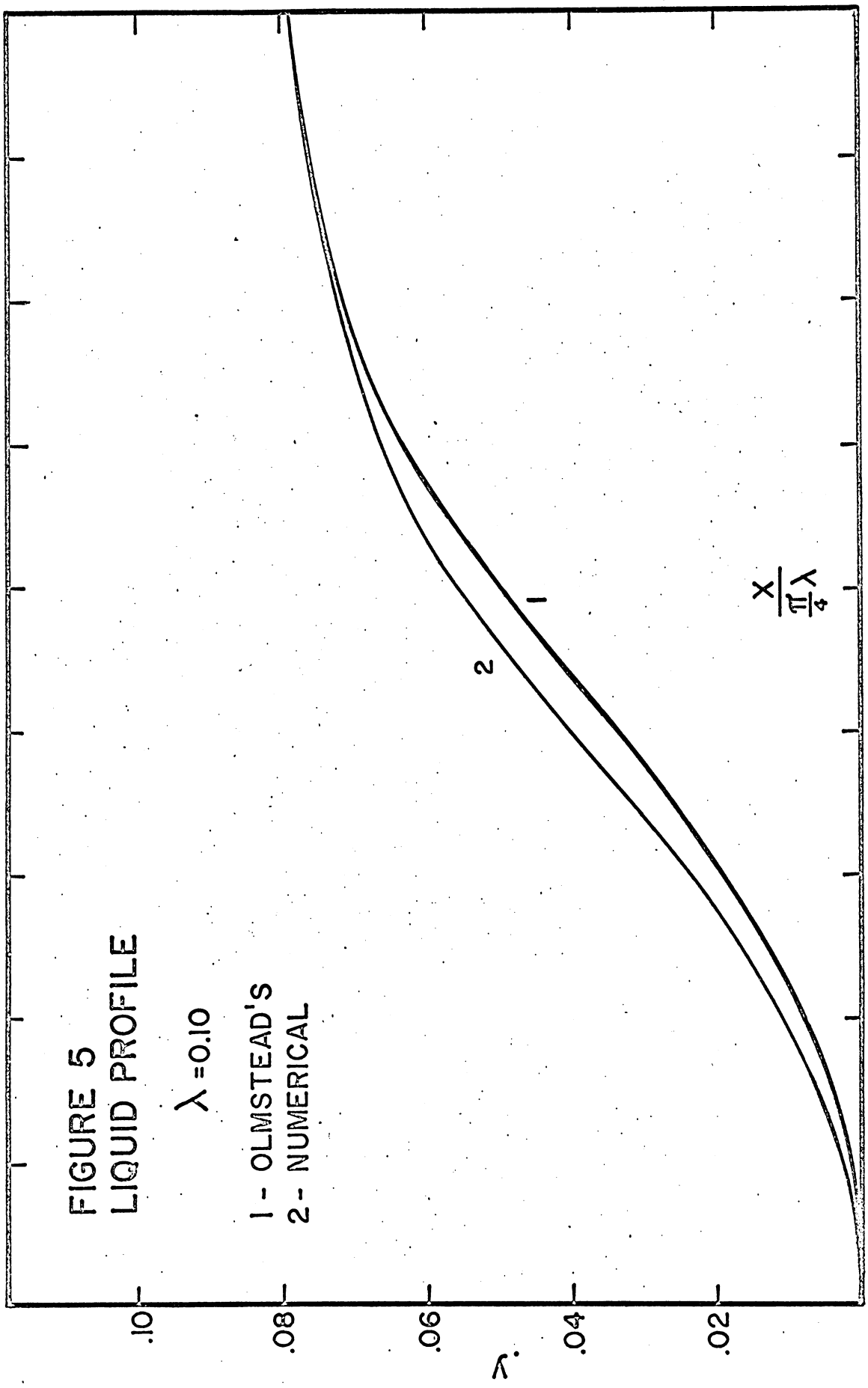
FIGURE 5
LIQUID PROFILE
λ =0.10
1 - OLMSTEAD'S
2 - NUMERICAL
y
.10
.08
.06
.04
.02
0
10
20
30
40
50
60
70
80
X/(π/4 λ)
1
2

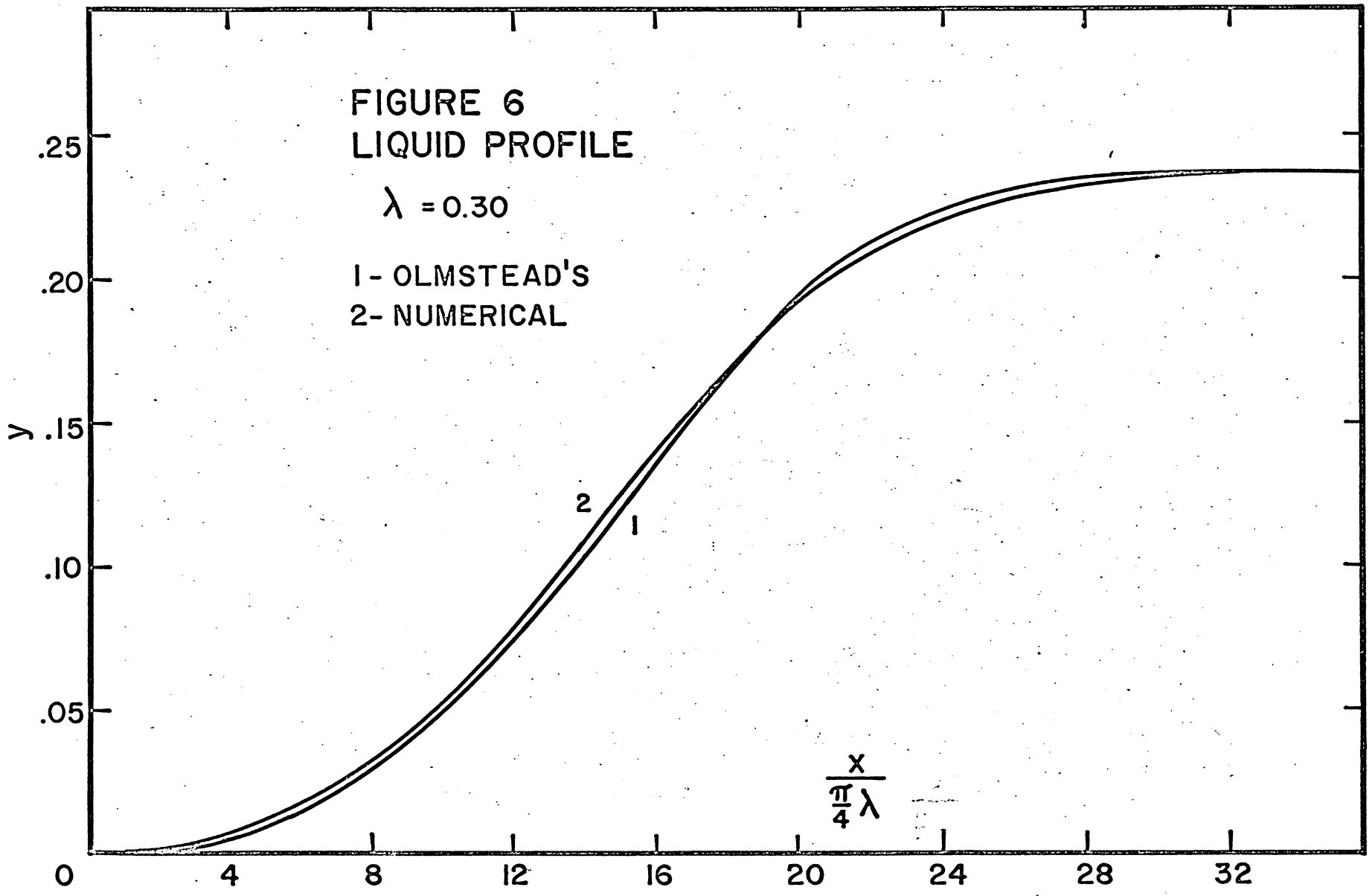
FIGURE 6
LIQUID PROFILE
λ = 0.30
1 - OLMSTEAD'S
2 - NUMERICAL
y
.25
.20
.15
.10
.05
0
4
8
12
16
20
24
28
32
2
1
x / (π/4 λ)

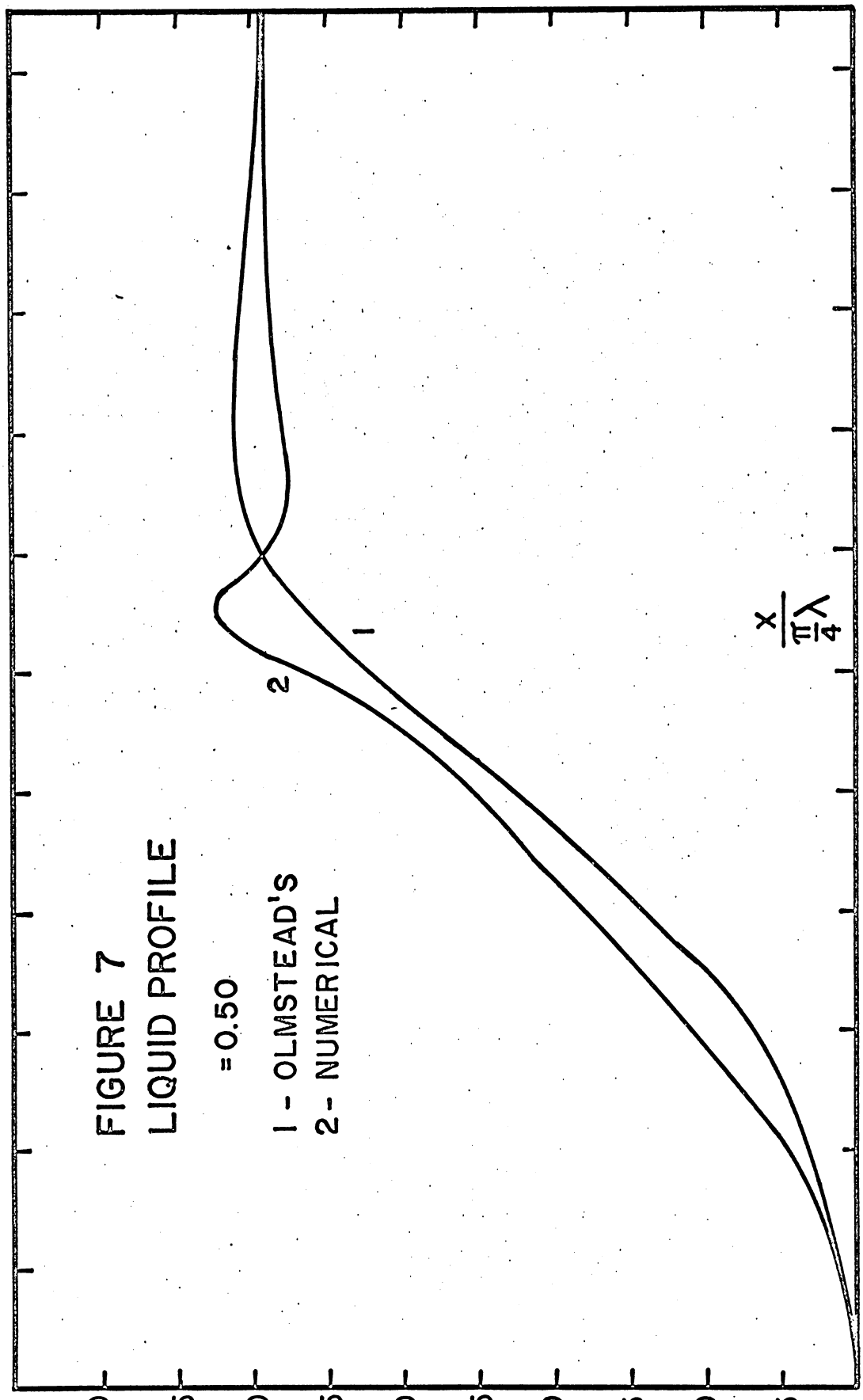
FIGURE 7
LIQUID PROFILE
=0.50
1 - OLMSTEAD'S
2 - NUMERICAL
1
2
y
.50
.45
.40
.35
.30
.25
.20
.15
.10
.05
0
2
4
6
8
10
12
14
16
18
20
22
$\frac{x}{\frac{\pi}{4}\lambda}$

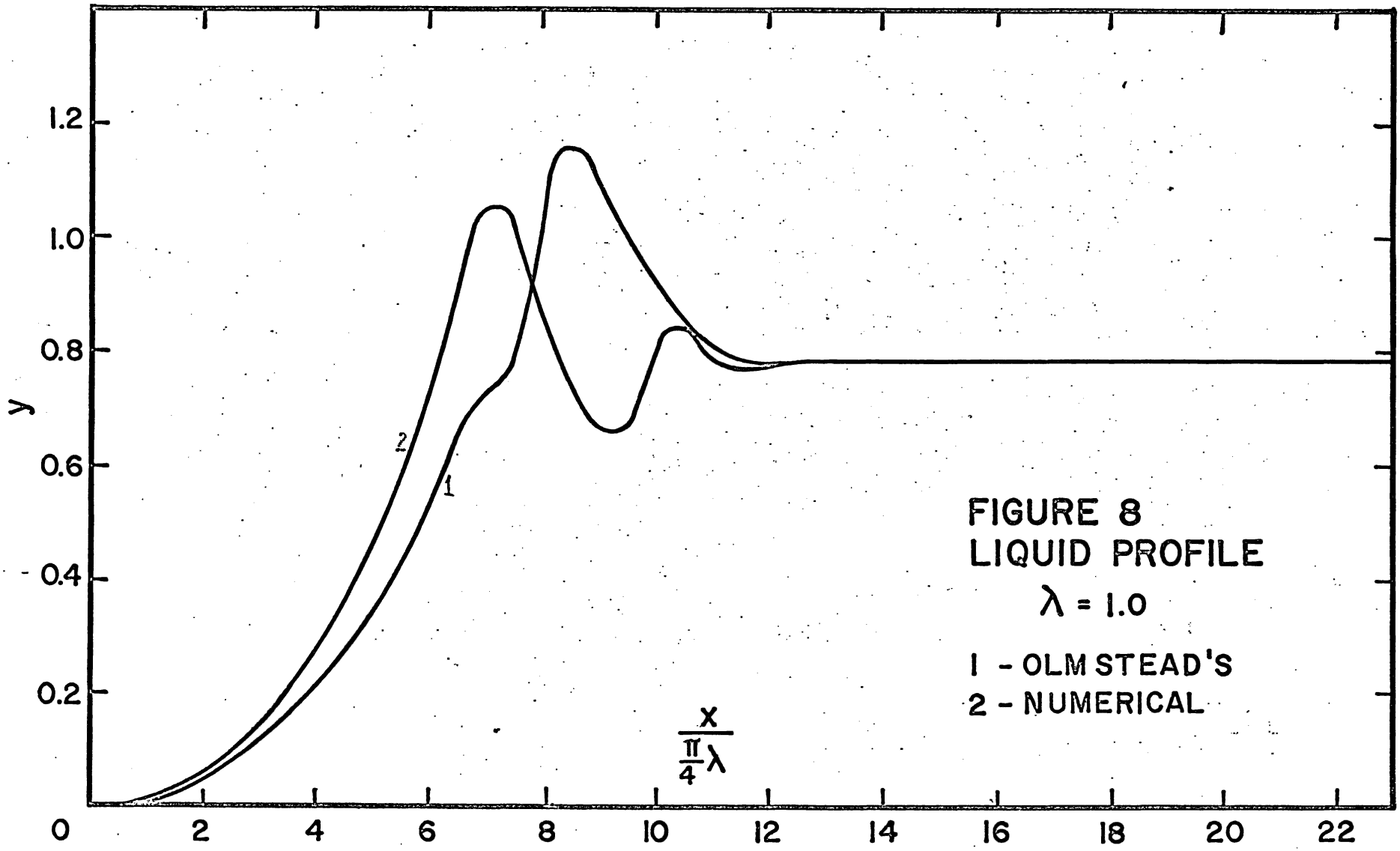

FIGURE 8
LIQUID PROFILE
$\lambda = 1.0$

1 - OLMSTEAD'S
2 - NUMERICAL

DISCUSSION OF RESULTS

A. Solution for the Liquid Profiles and Free Streamlines

1. Liquid Profile

Results presented in Figs. 5, 6, 7, 8 show that as the parameter λ is increased (i.e., for a given gas and liquid, the jet velocity V_j is increased) the depressions become deeper. For $\lambda = 0.5$, a small lip is discernible. And as λ is increased to a value of 1.0, a ripple emerges together with a lip which has become more pronounced.

2. Free Streamlines

For all values of λ, the position of the free streamline is below that of the flat plate solution, the deviation becoming greater as the value of λ is increased. However, as in the flat plate solution, all the free streamlines approach the line $Y = \pi/2$ asymptotically. For $\lambda = 1.0$, the free streamline dips down to such an extent that it goes below the line $Y = \pi/2$, but again approaches the flat plate solution at large values of X.

B. Comparison with Published Experimental Results

Banks and Chandrasekhara[1] have done an extensive experimental investigation on the penetration of a high-velocity gas jet through a liquid surface. The cavity depth, width and height of the lip were measured as functions of various independent variables such as the jet

velocity, liquid depth and a parameter H, defined as the finite height of the jet nozzle above the liquid surface. In this present paper, however, H has a value of infinity, compared to the range covered by Banks and Chandrasekhara of 0.10 to 1.0 ft. Because of this, quantitative comparisons between the numerical and the experimental results are not possible.

Qualitatively, however, photographs taken of experimental runs at low gas velocity agree with the numerical results. They also verify the appearance of a lip as jet velocity is increased and the existence of small ripples propagated from the cavity center.

C. Comparison with Olmstead's Analytical Solution

As in Olmstead's solution, results for $\lambda = 0.1$ and $\lambda = 0.3$ are characterized by the absence of lips. At $\lambda = 0.5$, however, a slight protuberance becomes discernible.

From Figs. 7 and 8, it can be seen that the shape of the liquid profiles differ from Olmstead's for values of λ equal to 0.5 and 1.0. For $\lambda = 0.5$, it can be observed that the numerical solution shows a lip which dips down more abruptly from its maximum height until it reaches a level below the original level of the liquid surface after which it slowly rises up. Olmstead's solution, on the other hand, exhibits a lip which descends very gradually from its maximum height and which reaches the level of the liquid surface at $X = \infty$. The profile for $\lambda = 1.0$ is markedly different from Olmstead's solution. Besides a lip, the presence of a ripple on the liquid surface is also evident.

Also of some physical importance is the ratio of cavity width (defined as the distance between the two lip peaks) to cavity depth. Listed below is a comparison of Olmstead's values with the numerical results.

λ	(Cavity width)/(Cavity depth)	
	Numerical	Olmstead's
0.5	26.4	31.5
1.0	14.5	17.5

D. Comparison of the Theoretical Thrust on the Liquid Surface with the Numerical Solution

A further check on the results may be made by comparing the thrust on the liquid surface with the theoretical value.

Let F_V = force exerted on the liquid surface per unit jet length.

Then

$$F_V = 2\int_0^\infty (P_L - P_{atm})\, dx$$

From Bernoulli's equation for the liquid:

$$P_L - P_{atm} = \rho_L g (y_0 - y) = \rho_L g \frac{b}{\pi}(Y_0 - Y)$$

$$F_V = 2\rho_L g \left(\frac{b}{\pi}\right)^2 \int_0^\infty Y_0 \left(1 - \frac{Y}{Y_0}\right) dX$$

The force F_v must also be equal to the initial momentum of the jet.

$$F_v = b\rho_G V_j^2$$

$$\left(\frac{\rho_L g b}{2\rho_G V_j^2}\right)\left(\frac{4}{\pi^2 Y_0}\right)\int_0^\infty \left(1 - \frac{Y}{Y_0}\right) dX = 1$$

$$Y_0 = \frac{\pi}{4}\lambda \qquad \lambda = \frac{2\rho_G V_j^2}{\rho_L g b}$$

$$\int_0^\infty \left(1 - \frac{Y}{Y_0}\right) dX = \pi$$

An error term may then be defined as:

$$\text{ERROR} = \frac{\left|\pi - \int_0^\infty \left(1 - \frac{Y}{Y_0}\right) dX\right|}{\pi} \times 100$$

This quantity can then be considered as a measure of the deviation of results from the theoretical. Below is a tabular representation of the ERROR term for both the numerical and Olmstead's methods.

λ	ERROR	
	Numerical	Olmstead's
0.1	2.7%	0.0%
0.3	3.2%	1.1%
0.5	3.5%	2.4%
1.0	5.1%	7.6%

The above figures indicate that using the theoretical thrust on the liquid surface as criterion for comparison of results, Olmstead's method has better accuracy at lower jet velocity (lower λ),while the numerical approach is more accurate at higher λ .

REFERENCES

1. Banks, Robert B. and Chandrasekhara, D. V., "Experimental Investigation of the Penetration of a High-Velocity Gas Jet through a Liquid Surface", J. Fluid Mech., V. 15, part 1, Jan. 1963, 13-34.

2. Birkhoff, Garrett and Zarantonello, E. H., Jets, Wakes, and Cavities, Academic Press Inc., New York, 1957.

3. Greenspan, Donald, "On a 'Best' Five-Point Difference Analogue of Laplace's Equation", J. Franklin Inst., V. 266, 1958, 39-45.

4. Olmstead, William Edward, "Depression of an Infinite Liquid Surface by a Two-Dimensional Incompressible Jet", Ph.D. Thesis, Northwestern University, June 1964.

5. Milne-Thomson, L. M., Theoretical Hydrodynamics, MacMillan and Co., Ltd., London, 1938.

6. Pai, Shih-I., Fluid Dynamics of Jets, D. Van Nostrand Company, Inc., New York,1954.

APPENDIX I-A

RESULTS FOR THE FREE STREAMLINES FOR $\lambda = 0.30$

X	Y
1.57080	∞
1.68861	6.12611
1.72788	4.55531
1.74751	4.16261
1.78678	3.76991
1.96350	3.25548
2.10879	2.98451
2.35619	2.67035
2.44259	2.59181
2.74889	2.33263
3.03949	2.19911
3.14159	2.15984
3.53429	2.04989
3.92699	1.95957
4.31969	1.91244
4.71239	1.87710
5.10509	1.85354
7.85398	1.82605
∞	1.80642

APPENDIX I-B

RESULTS FOR THE FREE STREAMLINES FOR $\lambda = 0.50$

X	Y
1.57079	∞
1.57115	11.78097
1.64004	4.71239
1.68438	4.31969
1.74923	3.92699
1.82189	3.53429
1.95099	3.14159
1.96350	3.13701
2.22038	2.74890
2.35619	2.61311
2.74436	2.35619
2.74889	2.33171
3.14159	2.20989
3.53429	2.14193
3.92699	2.07708
4.31969	2.03274
4.71239	2.00414
5.10509	1.98615
11.78097	1.96385
∞	1.96350

APPENDIX I-C

RESULTS FOR THE FREE STREAMLINES FOR $\lambda = 1.00$

X	Y
1.57080	∞
1.57116	10.99557
1.64004	5.10509
1.72608	4.31969
1.81398	3.92699
1.95923	3.53429
1.96350	3.51813
2.17940	2.95839
2.35619	2.95839
2.65025	2.74889
2.74889	2.69548
3.14159	2.51581
3.53429	2.39488
3.92699	2.31609
4.31969	2.28716
4.71239	2.30410
5.10509	2.33473
6.67588	2.36509
10.21017	2.35655
∞	2.35619

APPENDIX II-A

RESULTS FOR THE LIQUID PROFILE

$\lambda = 0.10$

X	Y
0.00000	0.00000
0.39270	0.00069
0.78640	0.00272
1.17809	0.00613
1.57080	0.01087
1.96350	0.01689
2.35619	0.02401
2.74889	0.03191
3.14159	0.03013
3.53429	0.04013
3.92699	0.05533
4.31969	0.06141
4.71239	0.06623
5.10509	0.06987
5.49779	0.07254
5.89049	0.07440
6.28318	0.07571
6.67588	0.07661
7.06860	0.07730
7.46129	0.07764
7.85398	0.07793
8.24668	0.07812
8.63938	0.07825
9.03208	0.07834
∞	0.07854

APPENDIX II-B

RESULTS FOR THE LIQUID PROFILE

$\lambda = 0.30$

X	Y
0.00000	0.00000
0.23562	0.00046
0.47124	0.00186
0.70686	0.00422
0.94248	0.00760
1.17810	0.01205
1.41372	0.01765
1.64934	0.02448
1.88496	0.03262
2.12058	0.04214
2.35619	0.05304
2.82743	0.07885
3.53429	0.12489
4.00553	0.15585
4.71239	0.19267
5.18363	0.20828
5.89049	0.22170
6.36172	0.22649
7.06858	0.23051
8.24668	0.23320
9.42478	0.23404
10.60288	0.23433
11.78097	0.23444
12.95907	0.23562
∞	0.23562

APPENDIX II-C

RESULTS FOR THE LIQUID PROFILE

$\lambda = 0.50$

X	Y
0.00000	0.00000
0.39270	0.00296
0.78539	0.01182
1.17810	0.02671
1.57080	0.04781
1.96350	0.07517
2.35619	0.10844
2.74889	0.14636
3.14159	0.18628
3.53429	0.22374
3.92699	0.25444
4.31969	0.28688
4.71239	0.35708
5.10509	0.42378
5.49779	0.39391
5.89049	0.37695
6.28319	0.38105
6.67588	0.38919
7.06858	0.39002
7.46128	0.39062
7.85398	0.39105
8.24669	0.39135
8.63938	0.39155
9.03208	0.39170
∞	0.39270

APPENDIX II-D

RESULTS FOR THE LIQUID PROFILE

$\lambda = 1.00$

X	Y
0.00000	0.00000
0.39270	0.00417
0.78540	0.01658
1.17810	0.03738
1.57080	0.06686
1.96350	0.10544
2.35619	0.15358
2.74889	0.20905
3.14159	0.25688
3.53429	0.34349
3.92699	0.46442
4.31969	0.61206
4.71239	0.77885
5.10509	0.90496
5.49779	1.06348
5.89049	1.00491
6.28319	0.86250
6.67588	0.75593
7.06858	0.66305
7.46128	0.66799
7.85398	0.79422
8.24668	0.84299
8.63938	0.78883

APPENDIX II-D

(continued)

X	Y
9.03208	0.77281
9.42478	0.77971
9.81748	0.76875
10.21018	0.76846
10.60288	0.76856
∞	0.78540